Large disparity between optical and fundamental band gaps in layered In_{2}Se_{3}

Wei Li, Fernando P. Sabino, Felipe Crasto de Lima, Tianshi Wang, Roberto H. Miwa, and Anderson Janotti

Phys. Rev. B **98**, 165134 — Published 23 October 2018

DOI: 10.1103/PhysRevB.98.165134

Large Disparity Between Optical and Fundamental Band Gaps in Layered In_2Se_3

Wei Li[a], Fernando P. Sabino[a], Felipe Crasto de Lima[a,b], Tianshi Wang[a], Roberto H. Miwa[b], and Anderson Janotti[a*]

[a] *Department of Materials Science and Engineering, University of Delaware, Newark, DE 19716 and*

[b] *Instituto de Física, Universidade Federal de Uberlândia, C.P. 593, 38400-902, Uberlândia, MG, Brazil*

(Dated: September 26, 2018)

Abstract

In_2Se_3 is a semiconductor material that can be stabilized in different crystal structures (at least one 3D and several 2D layered structures have been reported) with diverse electrical and optical properties. This feature has plagued its characterization over the years, with reported band gaps varying in an unacceptable range of 1 eV. Using first-principles calculations based on density functional theory and the HSE06 hybrid functional, we investigate the structural and electronic properties of four layered phases of In_2Se_3, addressing their relative stability and the nature of their fundamental band gaps, i.e., direct *versus* indirect. Our results show large disparities between fundamental and optical gaps. The absorption coefficients are found to be as high as those in direct-gap III-V semiconductors. The band alignment with respect to conventional semiconductors indicate a tendency to *n*-type conductivity, explaining recent experimental observations.

* janotti@udel.edu

I. INTRODUCTION

Chalcogenides form a large family of 2D layered materials with diverse electronic and optical properties, that includes metals[1], semiconductors [2, 3], and topological insulators [4]. As typical of 2D layered materials, their electronic and optical properties strongly depend on the number of layers, the layer stacking sequence, and how the atoms are arranged within each layer [5]. In_2Se_3 is a distinguished member of this family of compounds. It has been investigated for many technological applications, including solar cells [6], photodetectors [7–10] and phase-change memory devices [11, 12]. Extraordinary photoresponse in 2D In_2Se_3 nanosheets has been observed [9, 13], with key figures of merit exceeding those of graphene and other 2D materials based photodetectors; the reported photoconductive response extends into ultraviolet, visible, and near-infrared spectral regions. In_2Se_3-based phase-change memories have been demonstrated, exploring transitions between different polytypes with diverse electrical properties [11, 12]. More recently, ferroelectric ordering in 2D In_2Se_3 has also been predicted [14], creating prospects of room-temperature ferroelectricity with reversible spontaneous electric polarization in both out-of-plane and in-plane orientations. All these properties and potential applications are affected by or depend on the polymorphism of In_2Se_3. The ease of stabilizing In_2Se_3 in different crystal structures with diverse electronic and optical properties can be detrimental to photodetectors, yet it may be desirable for phase-memory devices where the involved structures must display disparate electrical properties.

Although In_2Se_3 has been studied for many years, the reports on crystal structure are rather confusing and even contradictory in many cases [15–17], with remarkable disagreements on atomic positions within the layers and layer stacking sequence. At least four phases have been reported (α, β, γ, and δ), with one of them being a 3D phase (labeled γ) and the others identified as layered phases. The layered structures are composed of five atomic layer Se-In-Se-In-Se sets, with strong covalent bonds within each quintuple layer and van der Waals interactions connecting neighboring quintuple layers. Among the layered phases of In_2Se_3, α and β, shown in Fig. 1(a) and (b), are the most prominent, with a reported $\alpha \rightarrow \beta$ transition temperature of 473 K [18].

The reported values for the band gap of layered In_2Se_3, either from optical absorption spectra [19–22] or calculated using first-principles methods based on the density functional

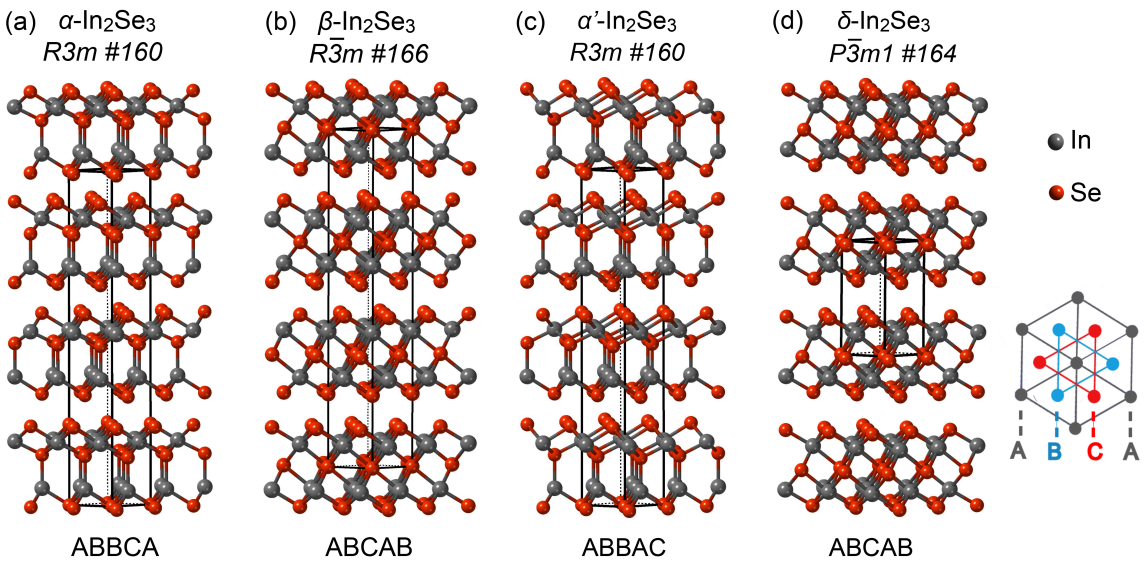

FIG. 1. Ball & stick model of the crystal structures of layered In_2Se_3 considered in the present work: (a) α-In_2Se_3, (b) β-In_2Se_3, (c) α'-In_2Se_3, and (d) δ-In_2Se_3. The space groups and the stacking within each quintuple layer are indicated. For α, β and α'-In_2Se_3, the hexagonal unit cells containing three formula units are displayed. For δ-In_2Se_3, the hexagonal cell shown is the primitive cell and contains two formula units.

theory [23, 24], vary from 0.55 eV to 1.5 eV, and the nature of the gap, i.e., direct or indirect, has often been overlooked. Here we perform hybrid functional calculations for the electronic and optical properties of four layered structures of In_2Se_3 (including the α and β structures shown in Fig. 1), paying special attention to the disparity between optical and fundamental band gaps. We compare the stability of the different phases through their formation enthalpies, calculate the real and imaginary parts of the dielectric functions, and determine optical absorption coefficients. We find that the layered structures all have indirect band gaps, with the lowest band gap of 0.17 eV and the highest of 1.35 eV. The calculated optical transition matrix elements reveal that the optical gap is significantly different from the fundamental band gap for two of the structures, and that the onset of optical absorption all occur at energies higher than 1 eV. We also compute the band alignment between the different phases, and find that the position of the conduction-band minimum (CBM) is relatively low with respect to the vacuum level, indicating a tendency for n-type conductivity for all the layered In_2Se_3 structures.

II. COMPUTATIONAL APPROACH

The calculations are based on the density functional theory [25, 26] and the screened hybrid functional of Heyd-Scuseria-Ernzerhof (HSE06) [27, 28] as implemented in the VASP code [29, 30]. The interactions between the valence electrons and the ions are described using projector augmented wave (PAW) potentials [31, 32]. To improve the description of the weak interaction between the quintuple layers of In_2Se_3, we adopted a van der Waals (vdW) correction according to the DFT-D2 method of Grimme [33]. The structures were optimized using a cutoff of 320 eV for the plane wave basis set, until forces on the atoms were lower than 0.005 eV/Å. The Brillouin zone was sampled using a Γ-centered 6×6×6 mesh of k-points for the primitive cells.

The structures of In_2Se_3 in Fig. 1(a)-(c) can be described by rhombohedral primitive cells containing one formula unit, while the structure in Fig. 1(d) is described by a hexagonal primitive cell with two formula units. These primitive cells are shown in Fig. 2. For the rhombohedral primitive cells we chose the following lattice vectors[34]:

$$\begin{aligned} \vec{a}_1 &= (b', a', a'); \\ \vec{a}_2 &= (a', b', a'); \\ \vec{a}_3 &= (a', a', b'), \end{aligned} \tag{1}$$

where the three vectors have the same length $a = \sqrt{2a'^2 + b'^2}$, and form an angle θ defined by θ=arccos $[(a'^2 + 2a'b')/a^2]$. In practice, the lattice parameters of the layered structures of In_2Se_3 are often reported using conventional hexagonal unit cells. Our choice of lattice vectors for the rhombohedral primitive cells makes it easy to express the lattice parameters of the hexagonal unit cells, a_{hex} and c_{hex} in terms of a and θ above. The lattice vectors of the hexagonal unit cells, containing three formula units, are given by:

$$\begin{aligned} a_{hex} &= a\sqrt{2(1 - \cos\theta)} \\ c_{hex} &= a\sqrt{3(1 + 2\cos\theta)}, \end{aligned} \tag{2}$$

The dielectric function along the in-plane a_{hex} direction ($\varepsilon_{hex,\parallel}$) and out-of-plane c_{hex} direction ($\varepsilon_{hex,\perp}$) are written as:

$$\begin{aligned} \varepsilon_{hex,\parallel} &= \varepsilon_{diag} - \varepsilon_{nondiag} \\ \varepsilon_{hex,\perp} &= \varepsilon_{diag} + 2\varepsilon_{nondiag}, \end{aligned} \tag{3}$$

where $\varepsilon_{nondiag}$ and ε_{diag} are the diagonal and nondiagonal elements of the dielectric tensor obtained using the rhombohedral primitive cells with the lattice vectors given by Eq. 1 [34]. The electronic band structures and dielectric functions were calculated using the HSE06 hybrid functional. The calculation of the optical transition matrix elements and the dielectric functions within the PAW method is described in Ref. 35. Test calculations using the GW method [36, 37] give band gaps that are systematically higher by only 0.1 eV. Contributions from excitons and phonon-assisted optical transitions to the absorption coefficient are expected to be relatively small and were not included in the present work.

III. RESULTS AND DISCUSSION

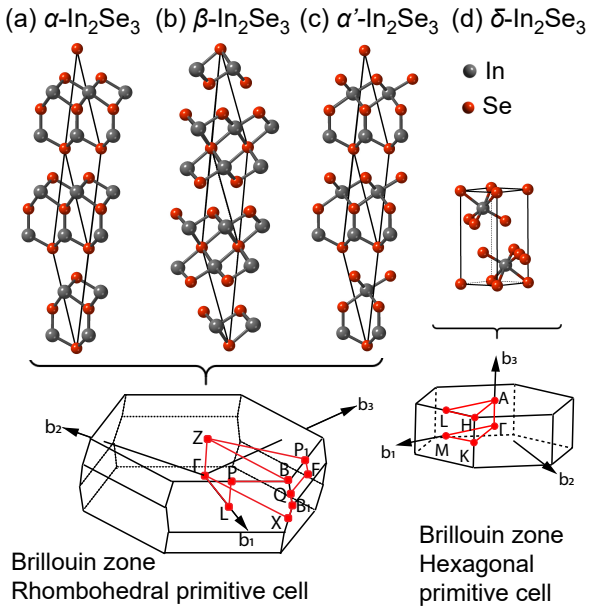

FIG. 2. Rhombohedral primitive cells for (a) α, (b) β, and (c) α'-In_2Se_3, and the hexagonal primitive cell for (d) δ-In_2Se_3. The Brillouin zones are shown at the bottom, along the k-paths used to plot the band structures.

A. Structure and stability of layered In_2Se_3

The crystal structures of layered In_2Se_3 are composed of sets of quintuple layers, Se-In-Se-In-Se, with each atomic layer containing only one elemental species arranged in a triangular

TABLE I. Calculated lattice parameters, a_{hex} and c_{hex}, and formation enthalpy ΔH_f for layered phases of In_2Se_3 using HSE06 and HSE06+vdW. Previous experimental and theoretical results, with references in square brackets, are also listed for comparison.

	a_{hex} (Å)	c_{hex} (Å)	ΔH_f(eV)
α-In_2Se_3			
HSE06	4.066	30.368	-3.982
HSE06+vdW	3.973	28.752	-3.109
Exp.	4.00	28.80 [17]	-2.858 [38]
	4.05	28.77 [15]	
Previous calc.	3.93	27.9 [23]	
β-In_2Se_3			
HSE06	3.978	29.890	-3.737
HSE+vdW	3.904	27.671	-3.071
Exp.	4.025	28.762 [39]	
	4.05	29.41[15]	
Previous calc.	4.00	29.04 [23]	
δ-In_2Se_3			
HSE06	3.978	10.195	-3.732
HSE06+vdW	3.902	9.322	-3.042
Exp.	4.01	9.64 [16]	
α'-In_2Se_3			
HSE06	4.003	30.279	-3.975
HSE06+vdW	3.975	28.785	-3.103

lattice. Within the quintuple layers, the atoms form strong covalent/ionic bonds, while the interactions between neighboring quintuple layers are weak and of the van der Waals type. The crystal structures in Fig.1 differ in the stacking within the quintuple layer and inter quintuple layers. The most studied phases of layered In_2Se_3 are the α and β shown in Fig. 1(a) and (b). In the α-In_2Se_3 structure, space group $R3m$, the Se-In-Se-In-Se atomic layers are stacked in the ABBCA sequence, where one of the In is fourfold coordinated in a tetrahedral environment, and the other is sixfold coordinated in an octahedral environment.

In the β-In_2Se_3, space group $R\bar{3}m$, both In atoms are sixfold coordinated in octahedral environments. In a variant of the α-In_2Se_3 structure, here labeled α', space group $R3m$, the Se-In-Se-In-Se atomic layers are stacked in the ABBAC sequence, where one of the In is fourfold coordinated, and the other is sixfold coordinated, as shown in Fig. 1(c). The δ-In_2Se_3 structure, space group $P\bar{3}m_1$, is a variant of the β-In_2Se_3, differing only in the stacking of the quintuple layers. While in β-In_2Se_3, each period along the out-of-plane direction (c_{hex} axis) contains three quintuple layers [Fig. 1(b)], in δ-In_2Se_3, each period along c_{hex} axis contains only one quintuple layer, as shown in Fig. 2(d).

The calculated lattice parameters of α, β, α', and δ-In_2Se_3, using both HSE06 and HSE06 with van der Waals correction (HSE06+vdW) are listed in Table I. HSE06 leads to a good agreement between theoretical and experimental results for in-plane lattice parameters a_{hex}, however the error in the out-of-plane lattice parameter c_{hex} exceeds 8.8% compared to the experimental value for the α structure. HSE06+vdW improves the description of c_{hex}, reducing the error to less than 3.0%.

The calculated formation enthalpies ΔH_f are also listed in Table I. ΔH_f is defined as:

$$\Delta H_f = E_{tot}(In_2Se_3) - 2E_{tot}(In) - 3E_{tot}(Se), \quad (4)$$

where $E_{tot}(In_2Se_3)$ are the total energies per formula unit of In_2Se_3 in the different crystal structures, $E_{tot}(In)$ and $E_{tot}(Se)$ are the total energies per atom of In and Se bulk phases. Using HSE06+vdW, we find that α-In_2Se_3 has the lowest formation enthalpy (-3.109 eV), followed by α', β, and δ-In_2Se_3. The calculated formation enthalpy of α-In_2Se_3 is in good agreement with available experimental data [38]. We note that vdW corrections systematically increase formation enthalpies by about 0.8 eV for the different phases of layered In_2Se_3.

B. Electronic structure of layered In_2Se_3

The calculated band structures of α, β, α', and δ-In_2Se_3, using the primitive cells and including the effects of spin-orbit coupling (SOC), are shown in Fig. 3. The path includes all the high symmetry k points in the irreducible part of the Brillouin zone. The four layered phases of In_2Se_3 display fundamental indirect band gaps, with highly dispersive conduction bands (small effective electron masses) derived from In s orbitals, and much less dispersive

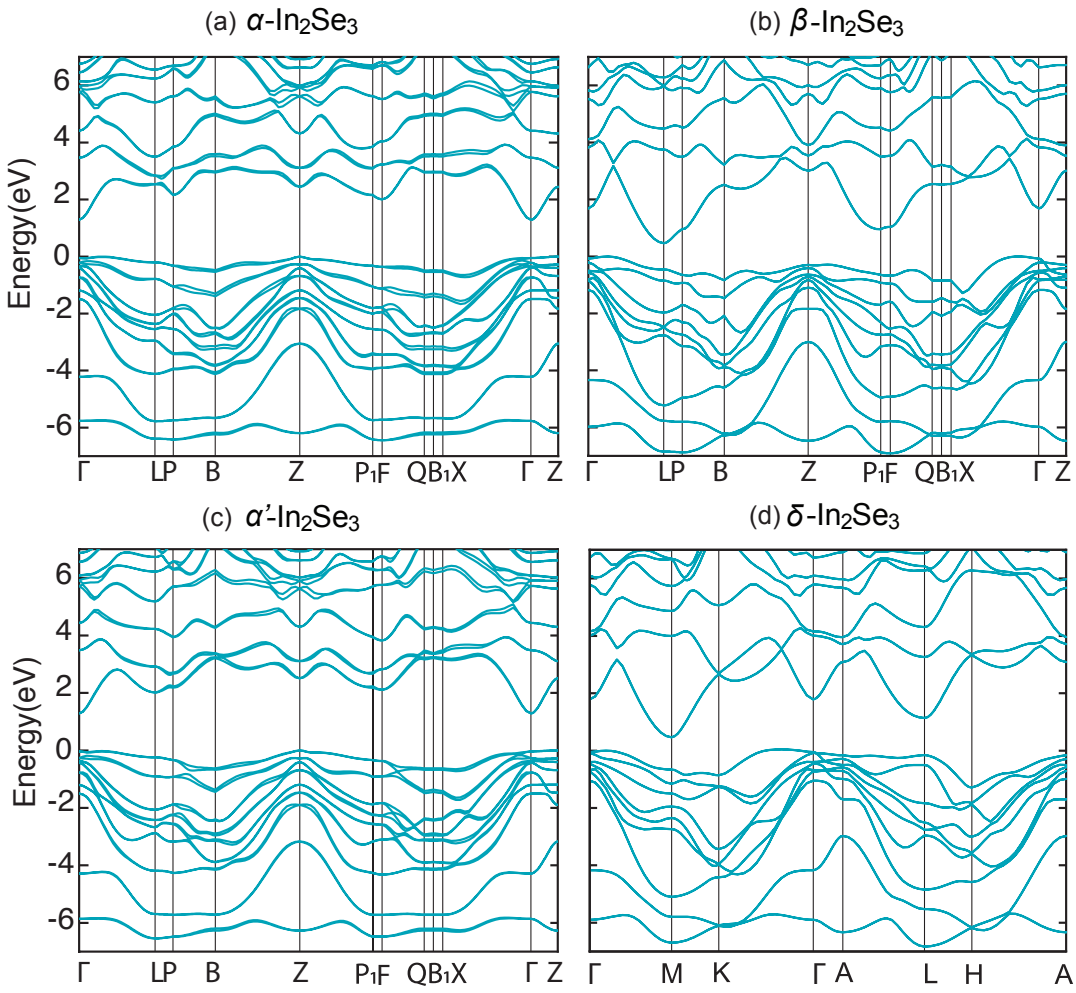

FIG. 3. Electronic band structure of α, β, α' and δ-In_2Se_3 using the primitive cells, and including effects of spin-orbit coupling (SOC). The valence-band maximum (VBM) is set to 0 eV.

valence bands derived mostly from Se p orbitals.

For α-In_2Se_3, the valence-band maximum (VBM) occurs along the Γ-L direction, while the CBM is located at Γ, with an indirect band gap of 1.27 eV. The indirect gap from Z to Γ is only 0.005 eV higher, while the direct band gap at Γ is 1.32 eV.

For β-In_2Se_3, the VBM occurs along the Γ-X direction, while the CBM is located at the L point, with a fundamental indirect band gap of 0.46 eV. The conduction-band edge at Γ is 1.22 eV higher than at L, and the valence-band edge at Γ is 0.08 eV lower than the VBM along Γ-X, so that the direct gap at Γ is 1.76 eV.

α'-In_2Se_3 has very similar lattice parameters, formation enthalpy, and band structure as α-In_2Se_3. The fundamental indirect band gap of α'-In_2Se_3 is 1.28 eV, i.e., only 0.01 eV

higher than that of α-In_2Se_3. The VBM occurs at the Z point and the CBM at Γ.

Finally, δ-In_2Se_3 has a small band gap of only 0.32 eV, with the VBM along the Γ-K direction and the CBM at the M point in the hexagonal Brillouin zone [Fig. 2(d)]. The direct gap at Γ is 1.84 eV.

Previous results of first-principles calculations for the band gap of In_2Se_3 vary in a wide range[23, 24]. The few reported band structures for bulk In_2Se_3 are nevertheless incomplete for the following reasons. First, the calculations were performed using the hexagonal unit cells, instead of the primitive cells. This may prevent a proper analysis of the direct *versus* indirect nature of the band gap since the Brillouin zone of the hexagonal unit cell is folded into that of the rhombohedral primitive cell. A direct gap in the Brillouin zone of the hexagonal cell may well involve distinct k points in the Brillouin zone of the primitive rhombohedral cell. Second, and more worrisome, the calculations for the hexagonal unit cells do not include all high-symmetry k points in the irreducible part of the Brillouin zone; they only include k paths in the in-plane direction passing through the Γ point. In fact, our calculations for the band structure of β-In_2Se_3 using the hexagonal unit cell show that while the VBM occurs at the Γ-K direction, the CBM occurs at the L point, i.e., not located in k paths in the in-plane direction passing through the Γ point [see the Brillouin zone in Fig. 2(d) for reference].

Based on full-potential linearized augmented plane-wave and local orbital (FPLAPW+lo) basis method and the modified Becke Johnson (mBJ) meta-GGA, an indirect band gap of 0.55 eV and a direct band gap at Γ of 1.5 eV were reported for β-In_2Se_3[24]. The authors argued that the calculated band gap was underestimated due to DFT band gap problem. However, the Becke Johnson (mBJ) meta-GGA approximation was designed to overcome this problem, giving band gaps in close agreement with experimental values. DFT-GGA calculations for α and β-In_2Se_3 resulted in indirect band gaps of 0.49 eV and 0.21 eV, while using the GW method, gaps of 1.25 eV and 0.7 eV were obtained[23]. However, the authors calculated the band structures using the hexagonal unit cells and only considered in-plane k-paths passing through the Γ point.

We also calculated the optical transition matrix elements between valence and conduction-band states for the four layered structures of In_2Se_3. For the α and α' structures, we find the lowest energy transition at Γ to be allowed and only slightly higher in energy than the fundamental indirect band gap.

For β-In_2Se_3, the minimum direct gap occurs at L, however, the corresponding transition matrix element, calculated as described in 35, is zero (forbidden transition). The matrix elements associated with optical transitions from the highest valence band to the lowest conduction band in the vicinity of the L point are negligibly small, and do not contribute to the absorption coefficient, so that the optical gap is associated with transitions from the second valence band to the conduction band at L. For δ-In_2Se_3, the optical gap is associated with a transition from the highest valence band and lowest conduction band at M.

These results show a large disparity between the fundamental and the optical gaps in the case of β and δ-In_2Se_3. In β-In_2Se_3, this disparity originates from the inversion symmetry of the crystal structure, making the lowest energy direct transition dipole forbidden. In δ-In_2Se_3, there is no inversion symmetry, and the disparity between the fundamental and optical gaps is attributed to the large difference between the indirect and direct band gaps.

C. Dielectric functions and absorption coefficients of layered In_2Se_3

The optical properties of layered In_2Se_3 are discussed based on the real and imaginary parts of the dielectric matrix, absorption coefficient and the optical transition matrix elements. To determine the optical band gap from the dielectric functions and the derived absorption coefficient we employed the tetrahedral method for the integration over the Brillouin zone, with a small Lorentzian broadening parameter of 0.001 eV. The calculations for the dielectric function were carried out for the rhombohedral primitive cells for α, β, and δ-In_2Se_3, and then converted to the hexagonal directions according to Eq. 3.

The real and imaginary parts of the dielectric function are shown in Fig. 4. Due to the hexagonal layered structure, we expect the dielectric function to be anisotropic, with nonzero components only in the out-of-plane ($\perp$) and in the in-plane ($\parallel$) directions.

For α, β, and α'-In_2Se_3, the real part of the dielectric tensor at zero energy (or frequency), is higher in the in-plane than in the out-of-plane direction, i.e., $\varepsilon_{\parallel}^{\infty} > \varepsilon_{\perp}^{\infty}$. This is expected since the electronic screening is stronger in the in-plane directions than in the out-of-plane direction due to the layered nature of the crystal structure. For the δ phase, we find $\varepsilon_{\perp}^{\infty} \approx \varepsilon_{\parallel}^{\infty}$, likely due to the alignment of the Se atoms connecting two neighboring quintuple layers, that favors the overlap of Se p orbitals across the quintuple layers, and the smaller distance

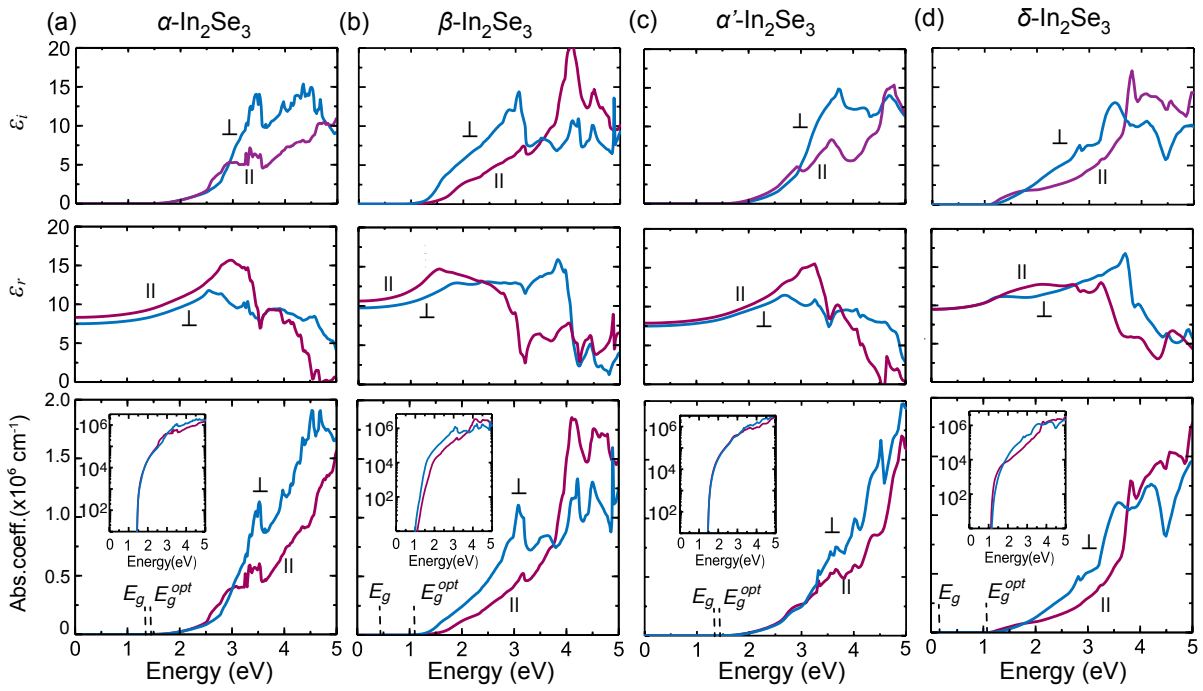

FIG. 4. Imaginary and real parts of frequency dependent dielectric function, ε_i and ε_r, for the layered phases of In_2Se_3. The calculated absorption coefficients are shown at the lower panels. The insets use logarithmic scale. The blue lines correspond to light polarization in the out-of-plane direction ($\perp$, along the c_{hex} axis), the purple lines correspond to light polarization in the in-plane direction ($\parallel$, along the a_{hex} axis). of the hexagonal cells of In_2Se_3.

between the quintuple layers.

The absorption coefficients were determined from the real and imaginary parts of the dielectric matrix and are shown at the lower panels in Fig. 4. For all the structures investigated, the amplitude of absorption coefficients are rather large for above band-gap excitations, i.e., exceeding 10^6 cm^{-1}, which are of the same order of magnitude as those in direct gap III-V semiconductors [40]. The optical absorption coefficients start increasing only at energies higher than 1 eV. Note that the optical band gap of α and α'-In_2Se_3 are similar to the fundamental band gap, because the small difference between the VBM and the of valence band edge at the Γ point. In contrast, the optical band gap of 1.27 eV for β-In_2Se_3 and 1.11 eV for δ-In_2Se_3 are much higher than the fundamental indirect gaps of 0.46 eV and 0.32 eV, respectively.

Optical absorption measurements of α and β-In_2Se_3 single crystals, where the β form was

obtained by heating α-In_2Se_3 crystals above 473 K in a furnace, revealed optical band gaps of 1.36 eV and 1.31 eV respectively[41]. Optical transmission measurements in α-In_2Se_3 films, deposited using thermal evaporation on glass substrates, indicated an indirect fundamental band gap slightly below the optical band gap of 1.37 eV [18]. Layered In_2Se_3 samples grown by vapor phase technique[17] have shown an onset in the absorption spectrum at 1.26 eV, with an estimated fundamental indirect gap of about 1.1 eV. The authors proposed a structure composed of quintuple layers with an unlikely truncated wurtzite crystal arrangement within each quintuple layer, where one Se atoms at the boundary is one-fold coordinated. We believe these results actually refer to α-In_2Se_3 based on the reported lattice parameters. Films of α-In_2Se_3 fabricated by ion-beam sputtering at 312 K from single crystals showed a band gap of 1.58 eV, determined from transmittance spectra [22]. More recently, a band gap of 1.46 eV for α-In_2Se_3 and 1.38 eV for β-In_2Se_3 were determined using photocurrent spectroscopy[42]. The authors noted that the β-In_2Se_3 films ($\sim$86 nm) were highly electrically conductive as a metal. All these results indicate optical band gaps above 1 eV, in agreement with our calculations.

Our calculations also offer some insights on the electronic structure of $(In_xBi_{1-x})_2Se_3$ even though we did not carry out explicit calculations for this system. Recent experiments have proposed that adding In to Bi_2Se_3 increases the band gap and reduces the Fermi level which is resonant in the conduction band of Bi_2Se_3, leading to a transition from a doped topological insulator to a trivial insulator with band gap over 1 eV [43]. However, it is unclear if the conduction-band edge in the $(In_xBi_{1-x})_2Se_3$ alloy is pushed up or if the ARPES measurements do not capture the k range where the band edges occur [43–45]. From our results, it is unlikely that alloying β-In_2Se_3 (band gap of 0.46 eV) with Bi_2Se_3 (0.22 eV) [46] would lead to fundamental band gaps larger than 1 eV as previously proposed [43].

D. Band alignments

Finally, we calculate the band alignment between the different structures of layered In_2Se_3. For β-In_2Se_3 and δ-In_2Se_3, we construct slabs with 9 quintuple layers and determine the averaged electrostatic potential of the middle quintuple layer with respect to the potential in the vacuum region of the slab. Then we take the VBM of bulk with respect to the averaged electrostatic potential in the bulk cell, which we equate to the averaged electrostatic potential

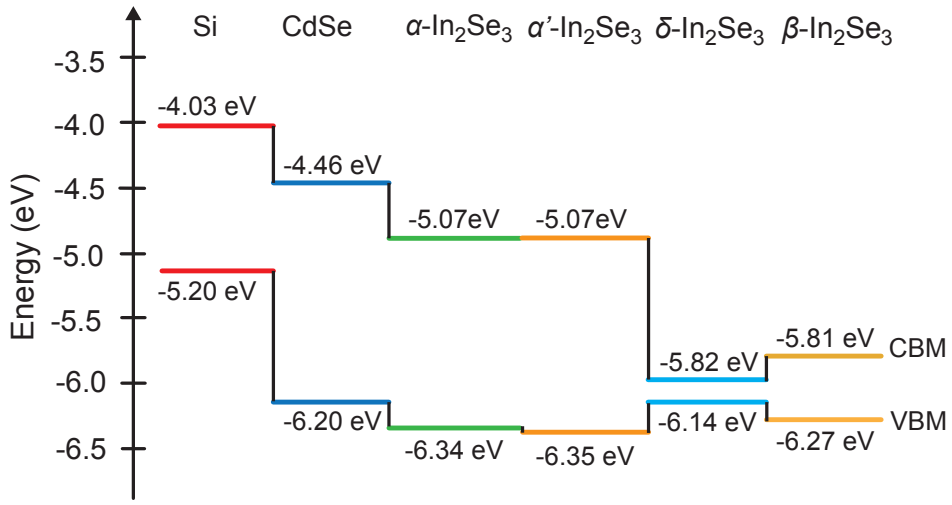

FIG. 5. Band alignment between α, β, α' and δ-In_2Se_3 and band edge positions with respect to vacuum level. The position of the band edges of CdSe and Si with respect to vacuum level, extracted HSE calculations from Ref. [49], are also shown for comparison.

in the middle of the slab, obtaining the VBM with respect to the vacuum level in each case.

In the case of α and α'-In_2Se_3, care should be taken to avoid charge transfer between the two interfaces in the slab due to the spontaneous polarization along the out-of-plane direction[14]. To overcome this problem, we build slabs for β-In_2Se_3 using the calculated equilibrium volumes of α-In_2Se_3 and α'-In_2Se_3. Assuming that the averaged electrostatic potential only depends on the volume, we can equate the potential in the slab of (strained) β-In_2Se_3 to that of α or α'-In_2Se_3, and then proceed to obtain the VBM of α and α'-In_2Se_3 with respect to vacuum.

The results of band alignments are shown in Fig. 5 and are compared to the values of the VBM and CBM for CdSe and Si from the literature [48, 49]. We note that the CBM of layered In_2Se_3 are lower than that of CdSe or Si, and lower than the standard hydrogen electrode potential (i.e., $\sim$-4.5 eV below the vacuum level [47]), implying that all the layered phases of In_2Se_3 will have a tendency for n-type conductivity. This is specially the case of β-In_2Se_3 and δ-In_2Se_3. This explains the recent measurements of photocurrent spectroscopy [42] where β-In_2Se_3 was reported to behave as a metal. It is also likely that the band gap of 1.38 eV determined from the onset in the photocurrent spectrum is larger than the

calculated optical gap of 1.23 eV in the present work due to the high density of electrons in the conduction band in the experiment, leading to a blue shift due to the Moss−Burstein effect. Finally, the VBM of the layered In_2Se_3 phases are almost aligned with that of CdSe, since they are derived mostly from Se $5p$ orbitals.

IV. SUMMARY

We report on the electronic structure and optical properties of layered In_2Se_3 using the HSE06 hybrid functional with vdW corrections. We find that the fundamental band gaps are indirect, and the optical gaps are all larger than 1 eV. In the case of β-In_2Se_3, which shares the same crystal structure of Bi_2Se_3, the fundamental band gap is only 0.46 eV, while the optical gap is 1.27 eV. The small fundamental band gap of β-In_2Se_3 is not expected to lead to alloys of In_2Se_3 and Bi_2Se_3 with gaps much larger than the gaps of the parent compounds as suggested in the literature. The calculated absorption coefficient are found to exceed 10^6 cm^{-1} and the onsets of optical absorption are overall in good agreement with experimental observations.

ACKNOWLEDGMENTS

We thank S. Law and Y. Wang for fruitful discussions. This work was supported by the National Science Foundation Faculty Early Career Development Program DMR-1652994. This research was also supported by the the Extreme Science and Engineering Discovery Environment supercomputer facility, National Science Foundation grant number ACI-1053575, and the Information Technologies (IT) resources at the University of Delaware, specifically the high performance computing resources.

[1] W. Choi, N. Choudhary, G. H. Han, J. Park, D. Akinwande, and Y. H. Lee, Mater. Today **20**, 116 (2017).

[2] S. Yang, C. Wang, C. Ataca, Y. Li, H. Chen, H. Cai, A. Suslu, J. C. Grossman, C. Jiang, Q. Liu, and S. Tongay, ACS Appl. Mater. Interfaces **8**, 2533 (2016).

[3] Z. Zheng, T. Zhang, J. Yao, Y. Zhang, J. Xu, and G. Yang, Nat. Nanotech. **27**, 225501 (2016).

[4] H. Zhang, C.-X. Liu, X.-L. Qi, X. Dai, Z. Fang, and S.-C. Zhang, Nat. Phys. **5**, 438 (2009).

[5] J. E. Padilha, H. Peelaers, A. Janotti, and C. G. Van de Walle, Phys. Rev. B **90**, 205420 (2014).

[6] H. Peng, D. T. Schoen, S. Meister, X. F. Zhang, and Y. Cui, J. Am. Chem. Soc. **129**, 34 (2007).

[7] N. Balakrishnan, C. R. Staddon, E. F. Smith, J. Stec, D. Gay, G. W. Mudd, O. Makarovsky, Z. R. Kudrynskyi, Z. D. Kovalyuk, L. Eaves, and A. Patanè, 2D Mater. **3**, 025030 (2016).

[8] T. Zhai, X. Fang, M. Liao, X. Xu, L. Li, B. Liu, and Y. Koide, ACS Nano **4**, 1596 (2010).

[9] R. B. Jacobs-Gedrim, M. Shanmugam, N. Jain, C. A. Durcan, M. T. Murphy, T. M. Murray, R. J. Matyi, R. L. Moore, and B. Yu, ACS Nano **8**, 514 (2014).

[10] J. O. Island, S. I. Blanter, M. Buscema, H. S. Van Der Zant, and A. Castellanos-Gomez, Nano Lett. **15**, 7853 (2015).

[11] H. Lee, D.-H. Kang, and L. Tran, Mater. Sci. Eng. C **119**, 196 (2005).

[12] B. Yu, S. Ju, X. Sun, G. Ng, T. D. Nguyen, M. Meyyappan, and D. B. Janes, Appl. Phys. Lett. **91**, 133119 (2007).

[13] W. Zheng, T. Xie, Y. Zhou, Y. L. Chen, W. Jiang, S. Zhao, J. Wu, Y. Jing, Y. Wu, G. Chen, Y. Guo, J. Yin, S. Huang, H. Q. Xu, Z. Liu, and H. Peng, Nat. Commun. **6**, 6972 (2015).

[14] W. Ding, J. Zhu, Z. Wang, Y. Gao, D. Xiao, Y. Gu, Z. Zhang, and W. Zhu, Nat. Commun. **8**, 14956 (2017).

[15] K. Osamura, Y. Murakami, and Y. Tomiie, J. Phys. Soc. Jpn. **21**, 1848 (1966).

[16] S. Popović, A. Tonejc, B. Gržeta-Plenković, B. Čelustka, and R. Trojko, J. Appl. Crystallogr. **12**, 416 (1979).

[17] J. Ye, S. Soeda, Y. Nakamura, and O. Nittono, Jpn. J. Appl. Phys. **37**, 4264 (1998).

[18] H. T. Ei-Shair and A. E. Bekheet, J. Phys. D: Appl. Phys. **25**, 1122 (1992).

[19] S. Marsillac, N. S. Mangale, V. Gade, and S. V. Khare, Thin Solid Films **519**, 5679 (2011).

[20] C.-H. Ho and Y.-P. Wang, Opt Mater Express. **3**, 1420 (2013).

[21] J. Clavijo, E. Romero, , and G. Gordillo, J. Phys. Conf. Ser **167**, 12016 (2009).

[22] I. V. Bodnar, Semiconductors **50**, 715 (2016).

[23] L. Debbichi, O. Eriksson, and S. Lebegue, J. Phys. Chem. Lett **6**, 3098 (2015).

[24] H. Ji, A. Reijnders, T. Liang, L. M. Schoop, K. S. Burch, N. P. Ong, and R. J. Cava, Mater. Res. Bull. **48**, 2517 (2013).

[25] P. Hohenberg and W. Kohn, Phys. Rev. **136**, B864 (1964).

[26] W. Kohn and L. J. Sham, Phys. Rev. **140**, A1133 (1965).

[27] J. Heyd, G. E. Scuseria, and M. Ernzerhof, J. Chem. Phys. **118**, 8207 (2003).

[28] J. Heyd, G. E. Scuseria, and M. Ernzerhof, J. Chem. Phys. **124**, 219906 (2006).

[29] G. Kresse and J. Hafner, Phys. Rev. B **47**, 558 (1993).

[30] G. Kresse and J. Hafner, Phys. Rev. B **48**, 13115 (1993).

[31] P. E. Blöchl, Phys. Rev. B **50**, 17953 (1994).

[32] G. Kresse and D. Joubert, Phys. Rev. B **59**, 1758 (1999).

[33] S. Grimme, J. Comput. Chem. **27**, 1787 (2006).

[34] J. Furthmüller and F. Bechstedt, Phys. Rev. B **93**, 115204 (2016).

[35] M. Gajdoš, K. Hummer, G. Kresse, J. Furthmüller, and F. Bechstedt, Phys. Rev. B **73**, 045112 (2006).

[36] M. S. Hybertsen and S. G. Louie, Phys. Rev. B **34**, 5390 (1986).

[37] M. Shishkin and G. Kresse, Phys. Rev. B **74**, 035101 (2006).

[38] C. Chatillon, J. Cryst. Growth **129**, 297 (1993).

[39] H. D. Lutz, M. Fischer, H. P. Baldus, and R. Blachnik, J. Less. Common. Met. **143**, 83 (1988).

[40] G. Stillman, V. Robbins, and N. Tabatabaie, IEEE Trans. Electron Devices **31**, 1643 (1984).

[41] C. Julien, A. Chlwy, and D. Siapkas, Phys. Status Solidi A **118**, 553 (1990).

[42] Q. Wang, L. Yang, S. Zhou, X. Ye, Z. Wang, W. Zhu, M. D. McCluskey, and Y. Gu, J. Phys. Chem. Lett **8**, 2887 (2017).

[43] J. Liu and D. Vanderbilt, Phys. Rev. B **88**, 224202 (2013).

[44] M. Brahlek, N. Bansal, N. Koirala, S. Y. Xu, M. Neupane, C. Liu, M. Z. Hasan, and S. Oh, Phys. Rev. Lett. **109**, 186403 (2012).

[45] L. Wu, M. Brahlek, R. V. Aguilar, A. V. Stier, C. M. Morris, Y. Lubashevsky, L. S. Bilbro, N. Bansal, S. Oh, and N. P. Armitage, Nat. Phys. **9**, 410 (2013).

[46] G. Martinez, B. A. Piot, M. Hakl, M. Potemski, Y. S. Hor, A. Materna, S. G. Strzelecka, A. Hruban, O. Caha, J. Novák, A. Dubroka, Č. Drašar, and M. Orlita, Sci. Rep. **7**, 6891 (2017).

[47] C. G. Van de Walle and J. Neugebauer, Nature **423**, 626 (2003).

[48] S. Ninomiya and S. Adachi, J. Appl. Phys. **78**, 4681 (1995).

[49] A. Grüneis, G. Kresse, Y. Hinuma, and F. Oba, Phys. Rev. Lett. **112**, 096401 (2014).